


2024

Human Second Metacarpal Nanocrystal Analysis

William Abramovich

DePaul University, wabramov@depaul.edu

Follow this and additional works at: <https://via.library.depaul.edu/depaul-disc>

 Part of the [Atomic, Molecular and Optical Physics Commons](#)

Recommended Citation

Abramovich, William (2024) "Human Second Metacarpal Nanocrystal Analysis," *DePaul Discoveries*: Volume 13, Article 3.

Available at: <https://via.library.depaul.edu/depaul-disc/vol13/iss1/3>

This Article is brought to you for free and open access by the College of Science and Health at Digital Commons@DePaul. It has been accepted for inclusion in DePaul Discoveries by an authorized editor of Digital Commons@DePaul. For more information, please contact digitalservices@depaul.edu.

Human Second Metacarpal Nanocrystal Analysis

Acknowledgements

This research used resources of the Advanced Photon Source, a U.S. Department of Energy (DOE) Office of Science user facility operated for the DOE Office of Science by Argonne National Laboratory under Contract No. DE-AC02-06CH11357. The authors thank Stuart R. Stock, Dept. of Cell & Developmental Biology, Northwestern Univ., Jun-Sang Park, Advanced Photon Source, Argonne National Laboratory, and U. Kierdorf, H. Kierdorf and S. Flohr, Univ. of Hildesheim, for their collaboration on this study. The author acknowledges the financial support of an Undergraduate Summer Research Program (USRP) grant from DePaul University's College of Science and Health.

Human Second Metacarpal Nanocrystal Analysis

William Abramovich*

Department of Physics and Astrophysics

Gabriela B. González Avilés, PhD; Faculty Advisor

Department of Physics and Astrophysics

ABSTRACT Female human bones dated to the 6th - 8th century CE were uncovered in Greding Germany after archaeologists discovered a medieval cemetery. Age-at-death estimates have been determined, and data from several techniques are currently being analyzed to learn more about these samples. The purpose of this project is to study the diaphysis (the long midsection) of the second metacarpal (mc2) bones excavated using wide-angle x-ray scattering data collected at beamline 1-ID of the Advanced Photon Source at Argonne National Laboratory. The diffraction data were refined using the Rietveld method to obtain lattice ('*a*' and '*c*') parameter values of the carbonated hydroxyapatite crystalline phase. One goal of the project was to investigate if there is a correlation between age-at-death and the lattice parameters. Another goal was to determine if '*a*' and '*c*' show spatial variation in the mc2 bones. The data were also compared to a modern mc2 sample.

INTRODUCTION

A recent study (Stock et al., 2022) used laboratory microComputed Tomography and synchrotron microComputed Tomography to examine human bone samples found in archaeological sites across Europe. The goal was to determine the age-at-death estimates of said samples and ascertain how diagenesis (degradation to a bone's microstructure) did or did not alter the bone microstructure.

The present project looked at samples from Greding, Germany using the Rietveld Method, a technique of crystallographic modelling which determines accurate lattice parameters from diffraction patterns acquired through Wide-Angle X-Ray Scattering (WAXS), a method utilized in Park et al., 2022.

Bone tissue consists of a collagen matrix containing $\sim 10^5$ nanocrystals of carbonated hydroxyapatite (cAp) per cubic micrometer. Hydroxyapatite's (HA) crystal structure is hexagonal with lattice parameters '*a=b*' and '*c*'. It contains calcium, oxygen, hydrogen, and phosphorus atoms. Figure 1 models hydroxyapatite. (Griggs, 2022)

Differences in '*a*' and '*c*' parameters within a second metacarpal (mc2) bone, and differences between samples could be due to the age-at-death, of which estimates were determined in Stock et al., 2022.

Park et al., 2022 found no correlation between '*a*' and '*c*' parameters and age-at-death and found that diagenesis (post mortem changes) occurred to such a degree that cAp crystallite size increased. This being said, the effects of diagenesis can fluctuate greatly amongst samples

* wabramov@depaul.edu

Research Completed in Summer 2023

found at the same site. Therefore, variations found in this analysis may be related to age-at-death.

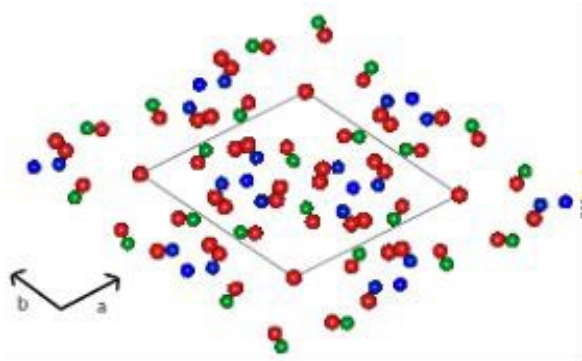


Figure 1. The hexagonal structure of hydroxyapatite comprised of calcium, oxygen, phosphorus, and hydrogen (not shown) atoms. The ‘*b*’ and ‘*a*’ axes are as shown and the ‘*c*’ axis points out of the page perpendicular to ‘*b*’ and ‘*a*’. The ‘*a*’, ‘*b*’, and ‘*c*’ parameters refer to the length of the respective axes. (Griggs, 2022)

METHODS

Rietveld Refinement

Rietveld refinement is a method used to derive accurate structural information about a polycrystalline material from its WAXS diffraction data. The method uses a least-squares iteration to fit calculated intensities to intensities observed in WAXS. It computes intensities based on peak shape and width and then compares those values to observed intensities (Sinha, 2023). This process utilizes Bragg's Law which relates the angles of incidence to the spacing between crystal lattice planes:

$$n\lambda = 2d\sin\theta \quad (1)$$

Bragg's Law is used to determine *d*-spacing. In this experiment, *n* is equal to 1, λ is equal to 0.173 Å, which is the wavelength of the x-ray beam, and θ is the scattering angle.

Equation 2 is then used to determine ‘*a*’ and ‘*c*’ based on the *d*-spacing calculated from Bragg's Law and their respective Miller indices (*hkl*). Miller indices are used to describe the orientation and location of crystal lattice planes within a crystal structure. Equation 2 is specific to hexagonal crystal structures. (Griggs, 2022)

$$\frac{1}{d^2} = \frac{h^2+k^2}{a^2} + \frac{l^2}{c^2} \quad (2)$$

WAXS Data Collection

WAXS data were measured using 71.676 keV ($\lambda = 0.173$ Å) x-ray photons and a $50 \times 50 \mu\text{m}^2$ beam size. The diffraction data were collected at beamline 1-ID of the Advanced Photon Source at Argonne National Laboratory (APS) (Park et al., 2022). The patterns were acquired across the whole sample at $\omega = 0^\circ$ and 180° (Fig. 2).

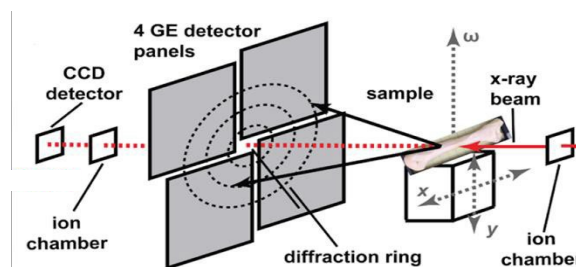


Figure 2 Depiction of the setup at Argonne National Laboratory (Park et al., 2022)

As shown in Figure 2, four two-dimensional GE detectors were used. Data from one horizontal (ge2) and one vertical detector (ge3) were analyzed.

This project analyzed a modern mc2 and ten Greding samples: HH48, HH66, HH71, HH135-1, HH136-2B, HH138_pl2, HH138_pl7, HH162-2, HH181, and HH223A.

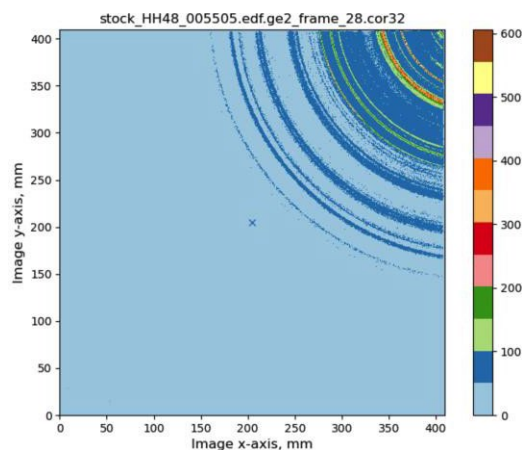


Figure 3. An example of a ge2 diffraction data image from the HH48 sample (frame 28) in which the color scale shows scattering intensity. Since this is 1 of 4 detector panels, only a quarter of the diffraction rings are visible.

The image seen in Figure 3 is one example of the 980 total frames collected at APS. The raw data were radially integrated. The patterns were acquired at 0° and 180° so that the average could then be taken to compensate for fluctuations in the center of mass resulting from the irregular bone cross-sectional shape (Stock et al., 2019).

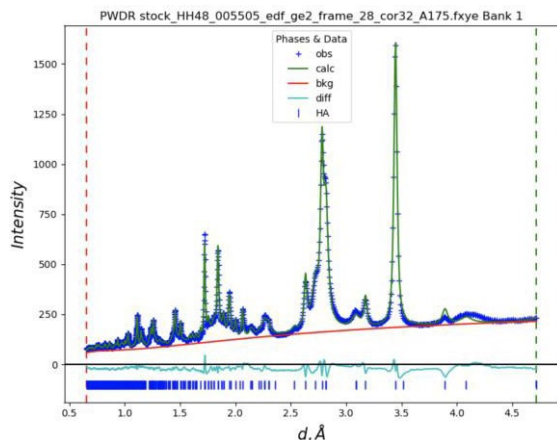


Figure 4. Integrated frame 28 depicting intensities from the HH48 sample. The blue crosses indicate the observed intensities, and the green line indicates the calculated intensities from the Rietveld refinement. The red line corresponds to the fitted background. The cyan line shows the difference between the calculated and observed intensities. The small vertical blue lines mark positions of the measured (hkl) reflections.

Rietveld refinement was then used to obtain lattice parameters for the ge2- 0° , ge2- 180° , ge3- 0° , and ge3- 180° diffraction patterns using the software package General Structural Analysis System (GSAS II) (Toby, B. H., & Von Dreele, R. B., 2013). Figure 4 shows an example of a typical Rietveld fit. It has been shown that the average of lattice parameters at 0° and 180° provides a precise value (Stock et al., 2019). Figure 5 shows how the lattice parameters were averaged. This process was done for each sample four times: ‘ a ’ for ge2 and for ge3, as well as ‘ c ’ for ge2 and ge3.

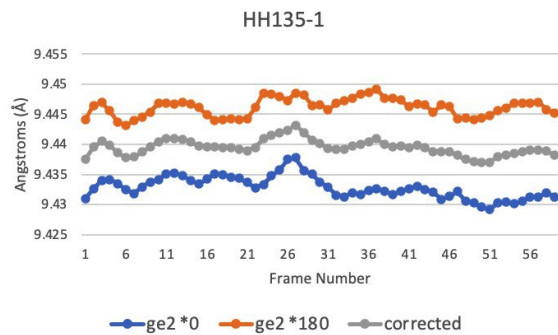


Figure 5. A chart showing ‘ a ’ parameters found from the ge2 frames for the HH135-1 sample. The blue line shows parameters found at 0° and the orange line shows parameters found at 180° . The grey line depicts the average between the two and charts the precise values.

Rietveld refinement was performed on all frames in which diffraction rings were visible.

RESULTS

The lattice parameters found from the 0° and 180° frames were averaged as shown in Figure 5, then those average values were plotted in the graphs shown in Figures 6, 7, 8, and 9 to visually compare the parameter variations between samples.

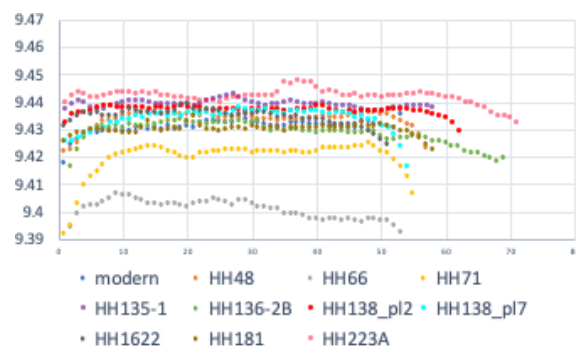


Figure 6. ‘ a ’ parameters from ge2 frames across all samples. The vertical axis refers to the calculated lattice parameter in angstroms (\AA), and the horizontal axis refers to the frame number.

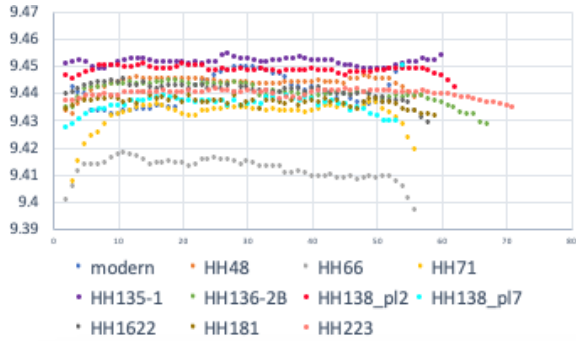


Figure 7. ‘a’ parameters from ge3 frames across all samples.

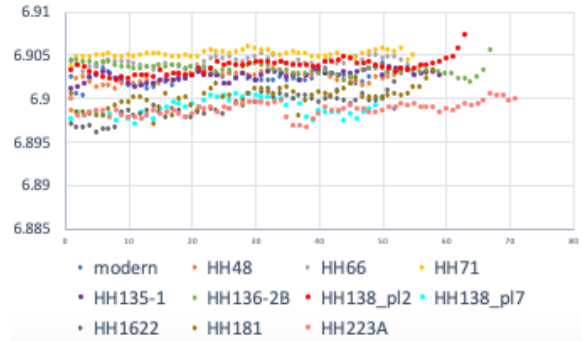


Figure 9. ‘c’ parameters from ge3 frames across all samples.

The graphs in Figures 6, 7, 8, and 9 are organized by detector (ge2 or ge3) panel and parameter (‘a’ or ‘c’) so that the differences between samples can be determined.

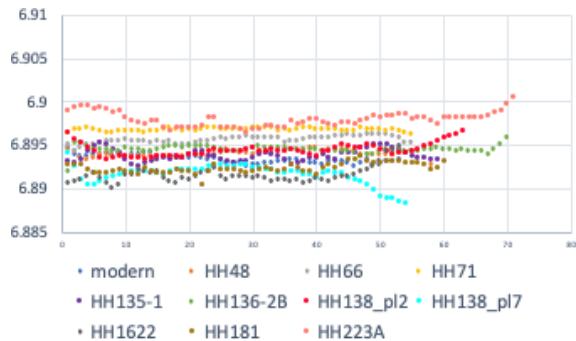


Figure 8. ‘c’ parameters from ge2 frames across all samples.

It is expected that these graphs look rather clustered. There were no major differences, except for the HH66 sample in both of the ‘a-parameter’ graphs. This means that there was something about the HH66 sample that caused the ‘a-parameter’ to be smaller than all the rest. The reason is currently unknown as this is an ongoing project and the age-at-death estimates for each of the samples are being withheld to avoid biases in the data analysis portion of this project. Eventually, the age-at-death estimates will be revealed for each sample, and we will see if there is any correlation between age-at-death and the lattice parameter data.

Sample	‘a’ ge2	σ	‘a’ ge3	σ	‘c’ ge2	σ	‘c’ ge3	σ
Modern	9.4309	2.6	9.4416	10.18	6.8934	0.47	6.9022	0.90
HH48	9.4320	10.5	9.4446	10.97	6.8940	0.35	6.9023	0.79
HH66	9.4000	4.6	9.4117	4.2	6.8955	0.40	6.9041	0.50
HH71	9.4196	6.7	9.4318	5.5	6.8967	0.18	6.9050	0.38
HH135-1	9.4393	1.6	9.4516	1.4	6.8938	0.67	6.9025	0.61
HH136-2B	9.4268	12.0	9.4400	5.4	6.8945	0.44	6.9032	1.3
HH138_pl2	9.4362	8.1	9.4484	1.8	6.8945	0.73	6.9036	0.86

HH138_pl7	9.4339	4.1	9.4359	3.4	6.8916	1.1	6.8989	0.99
HH162-2	9.4337	6.3	9.4409	3.8	6.8915	0.92	6.8991	2.0
HH181	9.4298	3.9	9.4365	2.3	6.8924	0.57	6.9001	1.2
HH223A	9.4422	2.7	9.4396	1.8	6.8980	0.83	6.8988	0.78

Table 1. Average ‘*a*’ and ‘*c*’ lattice parameters and standard deviations (σ) from their respective graphs. Average is in Angstroms (\AA) and standard deviation is in $\text{\AA} \times 10^{-3}$.

Table 1 shows all of the mean values for lattice parameters and is organized by sample, parameter (‘*a*’ or ‘*c*’) and detector panel (ge2 or ge3). The overall average ‘*a*’ parameter for the ge2 panel is 9.4295 \AA , the average ‘*a*’ parameter for the ge3 panel is 9.4385 \AA , the average ‘*c*’ parameter for the ge2 panel is 6.8942 \AA and the average ‘*c*’ parameter for the ge3 panel is 6.9018 \AA .

Some samples deviated from those averages by more than $5 \times 10^{-3} \text{ \AA}$, which is a significant difference since this is the threshold in which a Chi-Squared Test returns a *p*-value less than or equal to 0.05. Samples exhibiting such a difference in ‘*a*’ parameters in ge2 are HH66 ($-2.95 \times 10^{-2} \text{ \AA}$), HH71 ($-9.9 \times 10^{-3} \text{ \AA}$), HH135-1 ($9.8 \times 10^{-3} \text{ \AA}$), HH138_pl2 ($6.7 \times 10^{-3} \text{ \AA}$), and HH223A ($1.2 \times 10^{-2} \text{ \AA}$). These same samples show similar differences in ‘*a*’-ge3 (except for HH223A). No such differences are observed in ‘*c*’-ge2 or ‘*c*’-ge3.

DISCUSSION

In terms of the WAXS data that this project analyzed, Table 1 shows that the samples HH66, HH71, HH135-1, and HH138_pl2 all showed a significant difference when compared to the overall average ‘*a*’ lattice parameters found for both ge2 and ge3 detector panels. HH223A

showed a significant difference in ‘*a*’ parameters in the ge2 panel, but not ge3. No samples showed significant differences in ‘*c*’-ge2 or ‘*c*’-ge3.

The ‘*a*’ parameters for the ge2 (horizontal) detector had an overall range $4.2 \times 10^{-2} \text{ \AA}$, the ‘*c*’ parameters for the ge2 had an overall range of $6.5 \times 10^{-3} \text{ \AA}$. For the ge3 (vertical) detector the ‘*a*’ parameters had an overall range of $4.0 \times 10^{-2} \text{ \AA}$, while the ‘*c*’ parameters had an overall range of $6.2 \times 10^{-3} \text{ \AA}$. The ‘*a*’ values show a much greater range than those of ‘*c*’.

Currently, the samples are being analyzed with different techniques such as laboratory microComputed Tomography and synchrotron microComputed Tomography. All investigators working on this project are unaware of the age-at-death estimates that correspond to each sample so that an unbiased conclusion can be drawn about the postmortem collagen degradation after all of the samples have been analyzed.

Texture, crystallite size, and micro-strain analyses will be completed and compared to the lattice parameter results of the 11 samples. Rietveld analysis of the full set will give a comprehensive picture of the crystallographic variations in different samples and allow for a better understanding of the collagen degradation and of the effects of age at death.

ACKNOWLEDGEMENTS

This research used resources of the Advanced Photon Source, a U.S. Department of Energy (DOE) Office of Science user facility operated for the DOE Office of Science by Argonne National Laboratory under Contract No. DE-AC02-06CH11357.

The authors thank Stuart R. Stock, Dept. of Cell & Developmental Biology, Northwestern Univ., Jun-Sang Park, Advanced Photon Source, Argonne National Laboratory, and U. Kierdorf, H. Kierdorf and S. Flohr, Univ. of Hildesheim, for their collaboration on this study.

The author acknowledges the financial support of an Undergraduate Summer Research Program (USRP) grant from DePaul University's College of Science and Health.

REFERENCES

- Archaeology Museum Greiding. (n.d.). Outdooractive. Retrieved from <https://www.outdooractive.com/en/poi/altmuehltal/archaeology-museum-greiding/36102306/>
- Griggs, Kathryn (2022). X-Ray diffraction and structural analysis of shark vertebrae. *DePaul Discoveries*, 11(1), Article 9.
- Park, J.-S., Laugesen, M., Mays, S., Birkedal, H., Almer, J. D., & Stock, S. R. (2022). Intact archeological human bones and age at death studied with transmission x-ray diffraction and small angle x-ray scattering. *International Journal of Osteoarchaeology*, 32(1), 170–181. <https://doi.org/10.1002/oa.3053>.
- Sinha S. (2023). *The Crystal Structure of Hexagonal Molybdenum Oxynitride Hydride* [Master's Thesis, DePaul University]
- Stock, S. R., Laugesen, M., Birkedal, H., Jakus, A., Shah, R., Park, J.-S., & Almer, J. D. (2019) Precision lattice parameter determination from transmission diffraction of thick specimens with irregular cross sections. *Journal of Applied Crystallography*, 52, 40–46, <https://doi.org/10.1107/S1600576718017132>
- Stock, S. R., Mays, S., Turner-Walker, G., & Soriano, C. (2022). Microcomputed tomography (laboratory and synchrotron) of intact archeological human second metacarpal bones and age at death. *International Journal of Osteoarchaeology*, 32(1), 120–131. <https://doi.org/10.1002/oa.3049>.
- Toby, B. H., & Von Dreele, R. B. (2013). GSAS-II: the genesis of a modern open-source all purpose crystallography software package. *Journal of Applied Crystallography*, 46(2), 544–549. doi:10.1107/S0021889813003531